Volume 10
Number 11
November 2023
Pages 2927–3222

Environmental Science Nano

rsc.li/es-nano

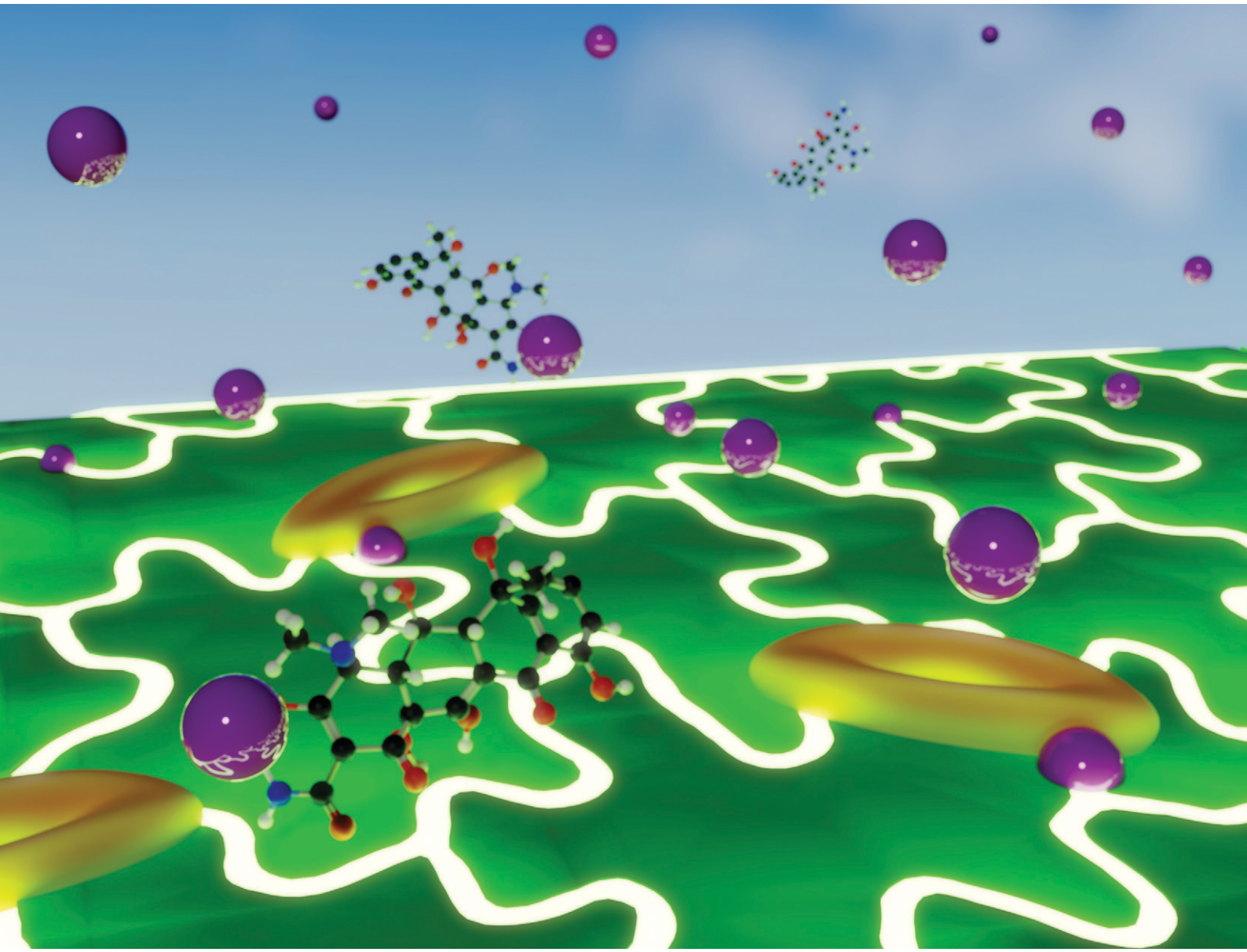

ISSN 2051-8153

ROYAL SOCIETY OF CHEMISTRY

PAPER

Jorge Pereira, Swadeshmukul Santra *et al.*
Targeted delivery of oxytetracycline to the epidermal cell junction and stomata for crop protection

Environmental Science Nano

ROYAL SOCIETY OF CHEMISTRY

PAPER

View Article Online
View Journal | View Issue

Cite this: *Environ. Sci.: Nano*, 2023, **10**, 3012

Targeted delivery of oxytetracycline to the epidermal cell junction and stomata for crop protection†

Jorge Pereira, *[ab] Daniela Negrete Moreno, [c] Giuliana Gan Giannelli,[d] Edwin Davidson, [ab] Javier Rivera-Huertas,[bd] Hehe Wang[c] and Swadeshmukul Santra *[abd]

Received 2nd March 2023,
Accepted 17th August 2023

DOI: 10.1039/d3en00140g

rsc.li/es-nano

Scalable targeted delivery methods are urgently needed for crop protection in modern agriculture. Herein, we report on the use of a novel borate-zinc nanoformulation (Bz) for the targeted delivery of Oxytetracycline (OTC). Fluorescence spectroscopy demonstrated the formation of the OTC–Zn complex when Bz is tank-mixed with OTC. Scanning electron microscopy (SEM) studies confirm that OTC changes the morphology of Bz residue after desiccation. SEM study was conducted on peach saplings with three different antimicrobial treatments, Bz, OTC and Bz–OTC. Results revealed that Bz alone or in combination with OTC preferentially deposited in the junction between epidermal cells as well as around the stomata. Fluorescence microscopy also confirmed that OTC was preferentially deposited in the same areas. In contrast, the OTC treatment produced sessile drop patterns with no special affinity for any leaf structures. Antimicrobial studies were conducted on OTC-resistant and OTC-sensitive *Xanthomonas arboricola* pv. *pruni* strain (XAP) strains. Results demonstrated moderate synergistic antimicrobial activity of Bz–OTC against the OTC-sensitive XAP strain and no loss in activity against the OTC-resistant XAP strain. To the best of our knowledge, this is the first report of targeted delivery of OTC to the epidermal cell junction and stomata using a micronutrient-based nanosystem.

Environmental significance

Conventional pesticides used for crop protection are usually applied through foliar sprays. However, most of the active ingredient never reaches its target and therefore disease control is not at the optimal level. To mitigate crop loss, farmers often maximize the frequency and the rate of application of pesticides. Long-term and frequent applications lead to chemical accumulation in soil, off-target toxicity, and promote the development of pesticide-resistant pathogens. Foliar antibiotics are currently used to protect many crops despite their low bioavailability due to limited chemical stability and lack of targetability to the leaf's most vulnerable areas. This work presents a rational design of a zinc and boron-based nanosystem that can deliver oxytetracycline to the stomata and epidermal cell junction while significantly increasing leaf surface coverage. These findings exemplify the potential of the nanosystem to be used as a tank-mix adjuvant to improve oxytetracycline performance and reduce the negative environmental impact of antibiotics.

Introduction

Globally, direct losses due to agricultural pests and pathogens range from 20 to 40%.[1] To ameliorate this, over 4 million tonnes of pesticides are utilized globally per year.[2–4] Even though pesticides are regularly used, it is estimated that less than 1% reach their target due to spray drift, runoff, and off-target deposition.[5] Their poor efficacy and constant use have led to environmental problems associated accumulation and run-off[6,7] and pesticide-resistant pathogens.[8,9] Among pathogens, phytopathogenic bacteria are estimated to collectively cause losses over 1 billion dollars annually.[10] The *Xanthomonas* spp. is one of the most economically impactful bacterial genus causing disease in a multitude of crops.[10,11]

An example of an economically important *Xanthomonas* subspecies is *Xanthomonas arboricola* pv. *pruni* (Xap), which causes bacterial spot on Prunus species worldwide.[12–14] Bacterial spot disease symptoms can be found on the tree's leaves, fruit, twigs, branches, and trunk.[14] Foliar disease

[a] *NanoScience Technology Center, University of Central Florida, Orlando, FL, 32826, USA. E-mail: jorge.pereira@ucf.edu, Swadeshmukul.Santra@ucf.edu*
[b] *Department of Chemistry, University of Central Florida, Orlando, FL, 32816, USA*
[c] *Edisto Research and Education Center, Clemson University, Blackville, SC, 29817, USA*
[d] *Burnett School of Biomedical Sciences, University of Central Florida, Orlando, FL, 32827, USA*

† Electronic supplementary information (ESI) available. See DOI: https://doi.org/10.1039/d3en00140g

symptoms include necrotic angular lesions, shot holes, yellowing, and in severe cases, defoliation. Early defoliation from bacterial spot infection causes weakened trees and impacts winter hardiness.[15] Normally, infected fruit is unmarketable due to necrotic spotted lesions. It has been reported that under optimal environmental conditions the disease can affect 100% of the fruit.[12,16] Twig infection from Xap leads to twig cankers, often observed in spring, and is considered a major inoculum source for leaf and fruit infection.[14,15,17] Bacterial spot of peach results in reduced orchard productivity, reduced quality and marketability of the fruit, and increased nursery cost.[12]

Bacterial spot management is challenging, mainly due to the susceptibility of most commercial peach cultivars, and the availability of limited chemical control options. Peach growers in the Southeastern United States rely heavily on routine sprays of copper and oxytetracycline (OTC) to manage bacterial spot, but disease incidence is still high especially when the environmental conditions are favourable (warm and rainy).[13,15,18] Moreover, management options are further complicated by the rise of oxytetracycline-resistant and copper-tolerant Xap strains.[15,17] Thus, novel chemical control options are in desperate need to better manage this disease.

Over the past decade, a significant amount of research has been done to demonstrate the potential of nanotechnology as an emerging tool for crop protection. A recent meta-analysis estimated that nanopesticides provide 31.5% increased efficacy against target organisms, 43.1% lower toxicity toward non-target organisms, and 41.4% reduced premature loss of active ingredients among other benefits, over conventional pesticides.[19] Due to the limited effectiveness and long-standing use of copper biocides in agriculture, copper-tolerant strains have emerged in several pathogenic bacterial species.[17,20–22] To manage these copper-tolerant pathogens several alternatives such as magnesium,[23–25] sulphur,[26–29] and transition metal-based[30–36] nanomaterials have been identified to conventional copper-based biocides. These alternatives possess have demonstrated plant compatibility, biological efficacy, and economical feasibility.[37]

The foliar disease cycle starts when the pathogen reaches the leaf surface. This is a complex environment inhabited by a multitude of other microbes, commonly known as phyllosphere.[38–40] In this ecosystem bacteria usually form aggregates or microcolonies in the boundary or junctions between epidermal cells, the stomata, the base of trichomes, and along the grooves of leaf veins.[38,39,41,42] *Xanthomonas* pathogens have been documented to populate the epidermal cell junction, surround the stomata, and colonize the stomatal cavity.[43–45] Since the leaf surface holds a limited amount of sugars and nutrients, it has been proposed that bacteria colonize and aggregate around "hot spots" that provide higher sustenance.[46–49] Due to the importance of these leaf structures for bacterial colonization in the phyllosphere, it might be possible to disrupt the bacterial infection cycle by preventing pathogens from occupying these vulnerable areas. Because the epidermal cell junctions are the most abundant structure on the leaf surface, it would be most effective to protect it against pathogens to prevent infections. Herein, we propose to target antimicrobials specifically to these vulnerable areas to prevent the formation of bacterial colonies and thereby reducing the number of viable bacteria (Fig. 1).

To target specific areas of the leaf tissue, it is necessary to understand its composition. The surface of the leaf is covered with a waxy cuticle made of long chain fatty alcohols, hydrocarbons, fatty acids, aldehydes, and terpenoids,[50,51] but it also contains proteins, polysaccharides, and fatty acid polyesters.[52] Underneath this waxy layer lies the epidermal cells which are protected by a cell wall that is mainly composed of cellulose, hemicellulose, and pectins.[53,54] The spatial distribution of polysaccharides in the leaf tissue can be visualized through immunolabeling using fluorescent monoclonal antibodies (MAbs). JIM7 is a MAb that recognizes a wide range of homogalacturonans (HGA). When JIM7 is tagged with a fluorophore, it clearly defines the junctions between leaf cells in the epidermis.[55,56] This occurs because pectin is located between plant cells to promote cell–cell adhesion, among other roles.[53,54,57] Due to their specificity, MAbs have been utilized to target gold nanoparticles to the stomata of *Vicia faba*.[58] Despite their effectiveness, MAbs would be challenging to use for crop protection because of their limited production, and stability and cost. Therefore, it is important to explore other alternate targeted delivery systems that are more robust, scalable and economical.

To deliver antimicrobials to the epidermal cell junctions the formulation must have affinity for pectin. It has been reported that boric acid covalently crosslinks through the formation of borate esters of rhamnogalacturonan II moieties.[59–62] Additionally, pectin has also been documented to crosslink due to the interaction between unesterified HGA moieties with divalent metal cations.[63,64] Given these interactions, it is logical to infer that a divalent metal-borate formulation would adhere and accumulate in the pectin-rich areas, such as the cell boundaries and stomata. A more pronounced effect can be obtained by reducing the size of the material to the nanoscale to increase its leaf cuticle penetration and surface interactions. Furthermore, borate and several divalent transition metal ions are essential plant micronutrients, which would enable the formulation to be assimilated and fertilize the plant over time. Therefore, it is hypothesized that metal-borate laden design of new materials can be utilized as a pectin-targeted delivery system. Such targeted delivery systems for agrochemicals will increase the efficacy of the agrochemicals delivered and reduce their negative environmental impact.

In this work, a borate–zinc nanoformulation was designed and developed to study its performance for delivering OTC to the epidermal cell junction and stomata of peach saplings. Dynamic Light Scattering (DLS), scanning electron microscopy (SEM), Fluorescence and Nuclear Magnetic Resonance (NMR) spectroscopy were utilized to study the interaction between the nanoformulation and OTC. The

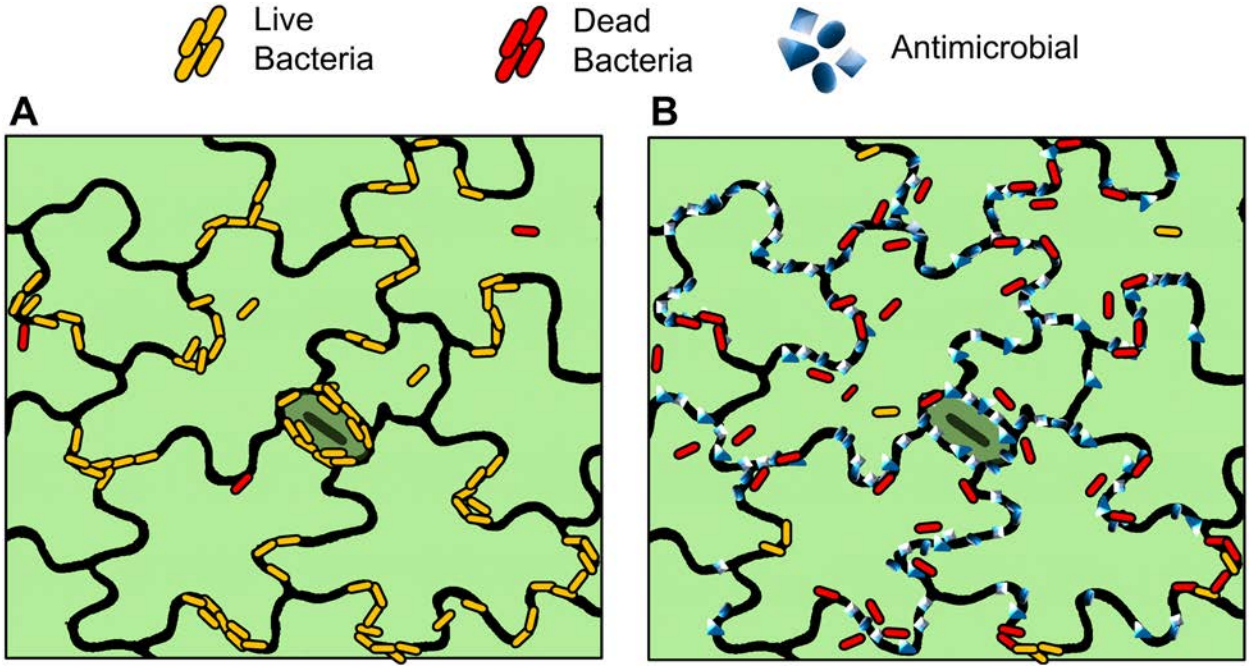

Fig. 1 A) Representation of bacteria colonizing the surface of a leaf, B) proposed strategy of protecting the leaf with antimicrobials that target the epidermal cell boundaries and stomata.

effects of Bz–OTC on the leaf surface coverage upon foliar spray were evaluated through digital image analysis of the residue on the leaves. The results were compared with their respective controls, Bz and OTC. SEM and Fluorescence Microscopy were utilized to map the spatial distribution of the Bz–OTC nanoformulation and OTC on the adaxial and abaxial surface of the leaf. Antimicrobial studies were performed to assess the compatibility of the Bz–OTC nanoformulation and their antimicrobial potency against OTC sensitive and resistant Xap strains in comparison to the controls.

Materials and methods

Synthesis of the nanoformulation

The nanoformulation was prepared through an aqueous precipitation method.[23,65] First, 7.42 g of boric acid (BA) (Fisher Chemicals) and 13.10 g of sodium gluconate (Acros Organic) were dissolved in 27.0 mL of 2.2 M sodium hydroxide solution. Separately, 17.85 g of zinc nitrate hexahydrate (Fisher Chemicals) were dissolved in 5.0 mL of DI water and slowly added to the boric acid solution while stirring at 600 rpm. Afterward, the pH was adjusted to 7.0 by adding 5.0 M sodium hydroxide solution at a rate of 1.43 mL min^{-1} with a peristaltic pump. The suspension was stirred for 24 hours before storage at room temperature. Hereafter, this nanoformulation will be referred to as Bz.

Dynamic light scattering studies (DLS)

First, Bz was filtered through a 0.2 μm PTFE syringe filter and then sonicated for 1 minute to separate particle aggregates. Afterwards, the suspension was studied using a Zetasizer ZS90 (Malvern Panalytical). DI water was selected as the dispersant and the scattering angle was set to 90°. The experiment was conducted in duplicate. The average and standard deviation of the Z-average, polydispersity index (PDI), and intensity distribution were reported.

Pesticide application to plants

Peach saplings (Sweet Dream/MP-29) were grown in an air-conditioned greenhouse at 28 °C. A hand-operated pump was utilized to spray the peach saplings with the treatments until the foliage was saturated with formulation (75.0 mL). The plants were rotated and sprayed at an angle of approximately 50 and −50° to cover both the adaxial and abaxial sides of the leaves, respectively. The saplings were left to air dry in the dark, to prevent photobleaching, until the formulations had completely evaporated from the leaves. Afterwards, leaves and tissue specimens were collected for fluorescence imaging and microscopy studies. Subsequently, plants were kept under natural day/night conditions and observed 72 hours after pesticide application for any signs of necrotic lesions or leaf burn to determine acute phytotoxicity.[35,66,67]

Bz was sprayed at a concentration of 800 μg of Zn mL^{-1}, while OTC was applied at 250 μg mL^{-1}. The combination of both pesticides (Bz–OTC) was applied also keeping the same concentration as the individual treatments (800 μg of Zn mL^{-1}; 250 μg of OTC mL^{-1}). OTC solutions were freshly prepared by dissolving oxytetracycline HCl (Alfa Aesar) in DI water for each study to prevent degradation. Peach saplings sprayed with DI water were used as the control.

Fluorescence spectroscopy of the formulations

Fluorescence studies were performed on a 96-well plate using a Tecan 200 M Infinite well plate reader with instrument parameters set at an excitation of 395 nm, scan range of 430–700 nm, Z-position of 20 000 μm and detector gain of 109. To better understand the interaction between Bz and OTC, they were mixed at the applied concentrations for 30 minutes. The mixture was then lyophilized (Labconco, FreeZone). The obtained powders were then resuspended separately in DI water and DMSO (Fisher Chemicals) at the applied concentrations.

Nuclear magnetic resonance (NMR) of the formulations

The lyophilized reaction mixtures were resuspended in D_2O (atomic% 99.8; Acros Organic) and sonicated before being analyzed at 400 MHz (Ultrashield Bruker) NMR.

SEM-EDS of the material

The Bz sample was prepared following the same method used in the DLS studies, as stated above. Afterwards, Bz, OTC, and their combination were adjusted to the application concentration and left to interact for 10 minutes. Then the formulations were diluted with DI water (Bz at 100 μg of Zn mL^{-1} and OTC at 31.25 μg mL^{-1}) first and then drop-casted on a silicon wafer. These samples were set to dry overnight within a silica gel desiccator.

The SEM images were obtained after 24 hours of dessication using a Zeiss Nvision 40 equipped with an In-Lens detector, operated at an acceleration voltage of 5 kV. Images were collected at 10 000× and 5000× magnification.

EDS mapping was performed on a Zeiss ULTRA-55 equipped with Noran 7 EDS system with Silicon Drift Detector.

Chemical residue analysis using fluorescence imaging technique

The coverage of residue on leaf surface was assessed using fluorescence imaging of treated leaves.[68] The analysis was done through setting a colour threshold of the recorded images.[69] Leaf specimens (n = 15) were collected from the saplings after the pesticides had dried up completely. The specimens were then placed on a black velvet mat and illuminated with a handheld UV light source (395 nm, Everbrite, LLC). Digital images were acquired at 17 cm above the specimen with a camera (13 MP; G6, LG Electronics Inc). The lighting and camera positions were kept constant for collecting digital images of all samples.

The digital images were processed using the ImageJ software. To measure the percentage of area covered with OTC, the images' colours were separated. Red colour threshold analysis was utilized to generate binary masks and calculate the total area of the leaves. Green colour threshold analysis was utilized to measure the area covered with OTC. The percentage of area covered was then calculated using the following equation:

$$\%\ \text{Covered with OTC} = [(\text{Pixels exceeding the green threshold})/(\text{Pixels exceeding the red threshold})] \times 100\%$$

Subsequently, the data was analyzed for statistical significance using a one-way ANOVA and Tukey *post hoc* ($P \leq 0.05$) using GraphPad Prism 9.4.1 (GraphPad Software Inc.).

Fluorescence microscopy of chemical residue on the leaves

Samples from treated peach plants were collected using a hand-held hole punch device. The leaf discs were then dry-mounted on clean glass slides and imaged using a confocal (fluorescence) microscope (BZ-X800, Keyence). Fluorescence images were acquired using a plan-apochromat (Keyence; 20×/0.75) objective and the GFP filter (Excitation 470/40 nm, Emission 525/50 nm).

SEM of chemical residue on the leaves

Leaf specimens were collected from treated plants and secured on the stage with carbon tape. The edges of the leaf were removed to avoid an excessive release of water vapor. No additional sample preparation was done to minimize distortion of the tissue or displacement of the residue. SEM images were acquired using a Hitachi 3000 tabletop microscope, operated at 15 kV using standard imaging mode at 600× magnification.

Checkerboard assay for the assessment of antimicrobial synergy

Five Xap strains were used (Table 1) for the assessment of antimicrobial synergy. All Xap strains were grown on nutrient agar (NA; Thermo Fisher Scientific) for 1–2 days before being transferred into 25 mL Erlenmeyer flasks with ~10 mL of nutrient broth (NB). Bacterial suspensions were then incubated overnight on an orbital shaker at 28 °C at 150 rpm. The next day, bacterial suspensions were adjusted to ~10^8 CFU mL^{-1} (OD_{600} = 0.1) with NB, and further diluted to 10^6 CFU mL^{-1} for all the antimicrobial studies.

To assess the interaction of OTC and Bz, the checkerboard assay was performed.[70,71] Briefly, Bz and OTC were combined in a sterile 96-well cell culture plate. Both treatments were serially diluted in opposite orientations of the plate to attain a final concentration gradient of 256–0.25 μg of Zn mL^{-1} for Bz and 128–2 μg mL^{-1} for OTC. Then the 10^6 CFU mL^{-1} suspension of bacteria was added to each well to achieve a final concentration of ~5×10^5 CFU mL^{-1}. Afterwards, the plates were covered with a sterile lid, sealed with parafilm and placed on an orbital shaker, set at 28 °C and 150 rpm. After 48 h of incubation, the OD_{600} was measured using a plate reader (Agilent BioTek, Epoch). For the OTC-sensitive Xap strain, the same protocol was used, except the OTC concentrations were amended to a lower concentration (4–

Table 1 Strains of *Xanthomonas arboricola* pv. *pruni* (Xap) used for the checkerboard assay

Strain	OTC S/R[a]	OTC resistance- threshold[b] (μg mL^{-1})	Year of isolation	Reference
2WF91	S	—	2018	17
M1	R	100	2017	15
F1	R	100	2020	15
R1	R	250	2020	15
T1	R	100	2017	15

[a] S: sensitive; R: resistant. [b] The OTC resistance-threshold was determined on NA amended with different concentrations of OTC.[15]

0.0625 μg mL^{-1} OTC). Each experiment included a growth control and run in triplicate.

The minimum inhibitory concentration (MIC) of OTC and Bz was determined for each replicate of the experiment for each Xap strain; OD_{600} = 0.15 was the threshold used to identify the MIC.

To evaluate the potential interaction between OTC and Bz, the fractional inhibitory concentration (FIC) index was calculated using the equation:[70]

$$FIC = (MIC_{OTC\ combination}/MIC_{OTC\ alone}) + (MIC_{Bz\ combination}/MIC_{Bz\ alone})$$

where $MIC_{OTC\ combination}$ and $MIC_{Bz\ combination}$ are the concentrations of OTC and Bz in the antimicrobial combinations that meet MIC threshold. Subsequently, the FIC values were used to assess synergistic (<0.5), antagonistic (>4), and additive or indifferent (0.5–4) interaction between OTC and Bz.[70]

Results and discussion

Material characterization

Bz appeared as a transparent liquid capable of light diffraction (Fig. S1A†). DLS studies revealed that Bz possesses a bimodal distribution with an average particle diameter of ~9 nm (Fig. S1B†). Interestingly, SEM images (Fig. 2A and D) reveal irregularly-shaped particles with diameter ranging 200–800 nm. This suggests that Bz particles of larger size are formed during the desiccation process.

When OTC was mixed with Bz, the Bz–OTC particles were in the micron-size (Fig. 2B and E, and S2†). Additionally, this composition seemed to arrange in branched structure as shown in Fig. S3.† OTC residue displayed a similar branched structure (Fig. 2C and F). Based on the morphological differences, it is apparent that OTC interacts with Bz.

EDS mapping of Bz and Bz–OTC (Fig. S2†) confirmed high signal originated from zinc, sodium, oxygen, and nitrogen, which suggests the presence of zinc nitrate and sodium nitrate. As expected, the signal from boron could not be reliably detected. The mechanism of the formation of larger sized particles of Bz and Bz–OTC during the drying process is complex and yet to be understood. Typically, larger-size crystalline particles are formed when a sessile drop of salt solution dries up.[72,73] During the drying process, other ions and molecules in the suspension influence the nucleation and growth processes as reported previously with surfactants,[74,75] small organic molecules,[76] macromolecules,[77–79] and cations.[78] The formation of submicron-sized Bz and Bz–OTC particles with different arrangements is likely due to the presence of nitrates, gluconates, borates and sodium ions.

It has been reported that the optical properties of OTC (absorption and emission) change when it is complexed with divalent metal cations (M^{2+}).[80–83] It is also reported that borate and boronic acids react to form borate complexes with 1,2 and 1,3 diols, carboxylic acids, amines, and imines, among others,[84–88] leading to changes in spectroscopic properties. Such changes in the spectroscopic properties formed the basis for developing chemical sensors[87,89–91] and quantifying analytes of interests.[92–97] Therefore, to corroborate the chemical interactions between OTC and Bz, the fluorescence spectroscopic studies were conducted in two different solvents, DI water and Dimethyl Sulfoxide (DMSO). Borate complexes and OTC are susceptible to hydrolysis in aqueous environment but not in DMSO. As shown in Fig. S4,† OTC fluorescence maxima appeared at 510 nm and 520 nm in DI water and DMSO, respectively when excited at 395 nm. In presence of Bz, the emission band of OTC broadened, and the peak maxima shifted to red by 10 nm in both solvents, which is significant. Furthermore, Bz increased the emission intensity of OTC by two orders of magnitude. The above change in OTC fluorescence characteristics confirms that Bz is interacting chemically with OTC where Zn is likely

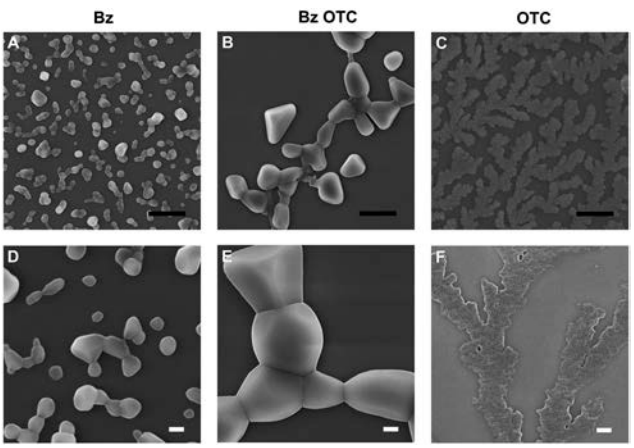

Fig. 2 SEM images of Bz (A and D), OTC (C and F), and Bz–OTC (B and E). Black scale bar set at 1 μm, white scale bar set at 200 nm.

forming a complex with OTC, altering its electronic properties. Broadening of OTC fluorescence band could be due to OTC–BA (in Bz) interaction that reduces OTC solubility leading to the formation of larger size particles. Similar changes in fluorescence have been reported for OTC–M^{2+} complexes.[80,83]

To further understand the chemical interaction between OTC and Bz, ^{11}B-NMR studies were performed in D_2O. Fig. S5† shows the ^{11}B-NMR spectra of the formulations. Bz and Bz–OTC demonstrate very similar spectra with a shallow peak around 18.64 ppm assigned to the uncharged trigonal planar [$B(OH)_3$] species[98] and broad peaks at 9.7, 5.11, and 1.0 ppm. The first and second broad peaks are assigned to the mono and bis 5-member cyclic borate esters, respectively.[98,99] The broad peak at 1.0 ppm represents the presence of the tetragonal species [$B(OH)_4^{1-}$], mono and bis 6-member cyclic borate esters.[98] Additionally, there are small peaks located at 4.4 and 3.2 ppm that are consistent with the presence of 5,6-member cyclic borate esters and mono 6-member cyclic borate esters from the hydroxy carboxylate moiety of gluconic acid.[98,100] ^{11}B-NMR spectra of BA and BA–OTC displays peaks at 19.28, 13.07, and 1.14 ppm characteristic of the penta-borate species.[100,101] ^{13}C-NMR of OTC and BA–OTC (Fig. S6†) corroborate that borate complexes are not being formed, but the ^{1}H-NMR demonstrates an up-field shift for OTC spectra when it is mixed with BA. This result correlates with the changes in fluorescence and suggests that BA alters OTC's solvation, which could have ramifications on its solubility leading to formation of larger size particles as well as accumulation on the leaf surface.

Considering the above findings, it is reasonable to say that Bz particles surface-immobilize OTC through OTC–Zn complexation in hydrophilic environment, producing sessile droplets. In subsequent experiments, this special property of Bz–OTC was exploited to target OTC to leaf structures that have an affinity for Bz.

OTC leaf surface coverage

Pesticide leaf coverage and deposition play an important role in protecting crops against microbes.[102–110] Traditionally, pesticide leaf coverage and spray patterns are studied through water-sensitive paper strips[111,112] or fluorescence imaging using tracer dyes.[68,69,113] Given the inherent fluorescence of OTC, its leaf surface coverage was assessed through fluorescence imaging. Fig. 3A–H represent the leaf surface covered with OTC based on its green fluorescence. The recorded green emission from DI and Bz treated leaves constitutes a small percentage of the total leaf surface area (Fig. 3I and J) and are attributed to high intensity light reflection that likely originated from uneven leaf surface. OTC treated leaves showed a droplet pattern with more confluent coverage near the tip and edges of the leaf. Bz–OTC treated leaves displayed a uniform coverage in comparison to the OTC treatment. Moreover, Bz–OTC coverage area is about 2× than that of OTC on both the abaxial and adaxial sides of

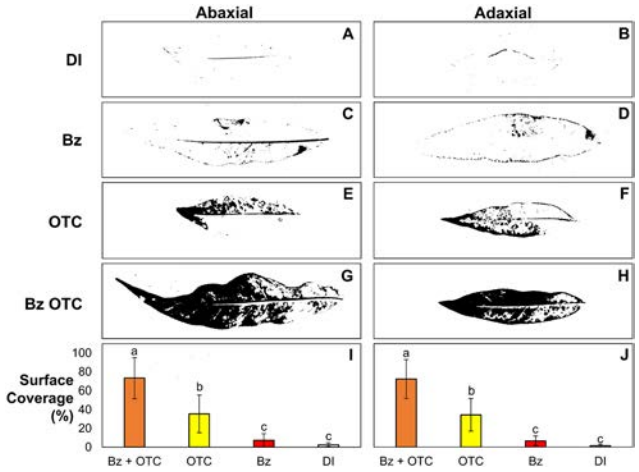

Fig. 3 Representative binary images generated through green colour threshold analysis (ImageJ) from digital images of treated peach leaves under UV/blue light (A–H). The shaded area denotes the pixels exhibiting green fluorescence over the threshold. Leaf surface covered in OTC represented as surface coverage % of the abaxial (I) and adaxial (J) sides of treated peach leaves. Error bars indicate standard deviation. A *p*-value of 0.05 was used for Tukey's *post hoc* analysis; different letters were assigned to statistically different groups.

the leaves (Fig. 3I and J). Previous studies showed that an increase in pesticide coverage leads to better biological efficacy.[39–41,49,114] Agriculture extension agents commonly recommend growers to use specialized nozzles, mist sprayers, or fans to enhance leaf coverage of agrochemicals in an effort to improve use efficacy.[115,116] This study shows that by mixing Bz with OTC, it is possible to achieve better disease management using traditional foliar spray equipment.

Microscopy analysis of chemical residue on the leaves

Scanning electron and fluorescence microscopy studies of the chemical residue on the leaves were performed to assess the microscopic distribution of the deposited formulations. SEM images of the treated leaves (Fig. 4A–H) adeptly shows the deposition of inorganic residue due to the difference in conductivity between the leaf tissue and the deposited inorganic material. SEM/EDS mapping of Bz treated leaves (Fig. S7†) correlate the presence of Zn, N and Na to the light grey residue. Bz and Bz–OTC treated leaves demonstrated similar deposition pattern on the adaxial and abaxial sides (Fig. 4B, C, F and G). The adaxial side of the leaf showed residue deposition almost exclusively at the epidermal cell junctions, leaving the outer periclinal surface of the epidermal cells mostly uncovered (Fig. 4F and G). Furthermore, Bz and Bz–OTC were preferentially deposited around the stomata on the abaxial surface of the leaf. The epidermal cell junction and stomata areas are prone to bacterial colonization requiring better protection, while the outer periclinal surface is rarely populated by bacteria. Therefore, this unique spatial distribution is promising for disease control. The spatial distribution of OTC residue was

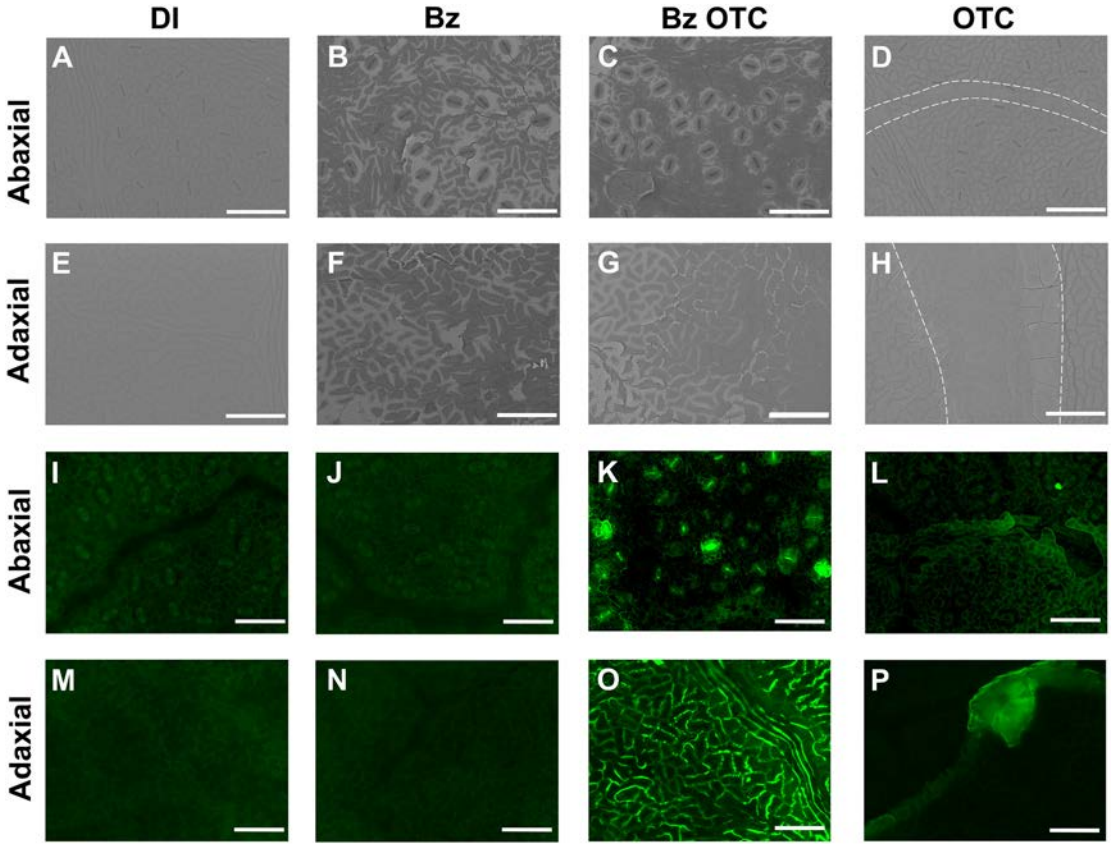

Fig. 4 SEM images of chemical residue on the abaxial (A–D) and adaxial side (E–H) of the peach leaves. Inorganic residue appears light gray (B, C, F and G) against the background. OTC residue is delineated with dashed lines (D and H). Fluorescence microscopy images of the chemical residue on the adaxial (I–L) and abaxial side (M–P) of the peach leaves. Inorganic residue lacks fluorescence at the excitation (I, J, M and N), while OTC residue fluoresces green (K, L, O and P). Bright fluorescent stomata are encircled in the abaxial Bz OTC residue (K). The scale bar was set to 100 μm.

assessed through fluorescence microscopy. Contrary to the other treatments, the residue on OTC-treated plants exhibited a "coffee ring" pattern,[72,79,117,118] forming a large crust on the edges of the droplet, with no affinity for any

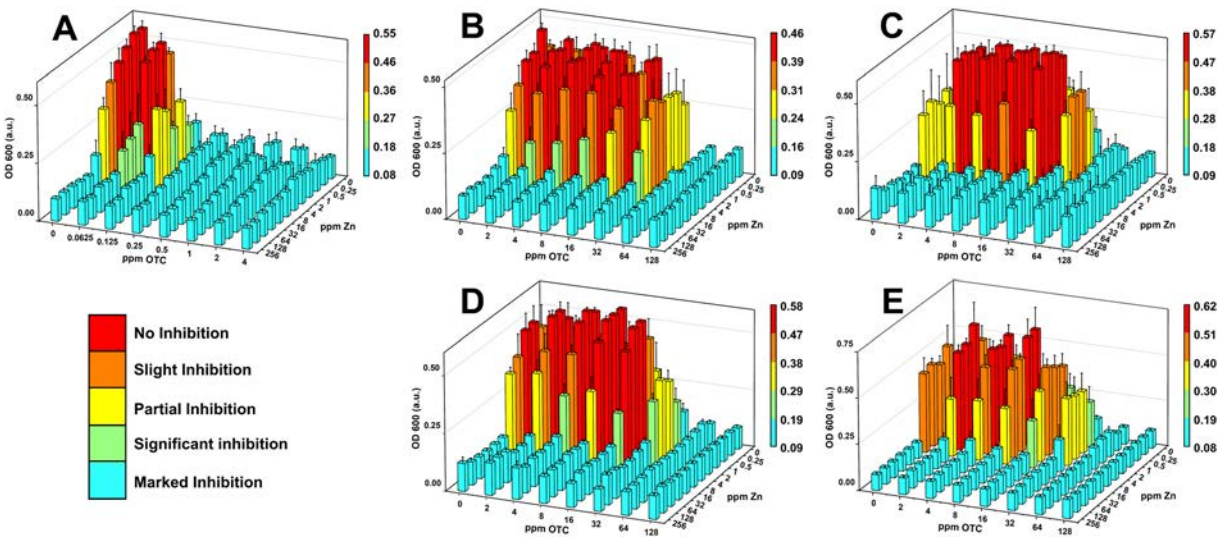

Fig. 5 Quantification of bacterial growth for each of the four OTC-resistant (B: R1, C: T1, D: M1, and E: F1) and one OTC-sensitive (A: 2wf91) Xap strains in response to different concentrations and combinations of Bz and OTC. The OD_{600} was measured to quantify bacterial growth after 48 hours of incubation and represented using a heat scale to facilitate visualisation. Values next to the heat scale represent the threshold values for each level. The error bars represent the standard error of the mean.

Table 2 The minimum inhibitory concentration (MIC) and fractional inhibitory concentration (FIC) index of OTC and Bz in the checkerboard assay

OTC resistance phenotypes (no. of bacterial strains)	MIC (μg mL^{-1})		FIC	
	$MIC_{OTC\ alone}$	$MIC_{Bz\ alone}$	Best $MIC_{OTC\ combination}$ & $MIC_{Bz\ combination}$[a] (ppm)	Mean[b]
OTC sensitive (n = 1)				
2WF9	0.125–2	8–16	0.0625 & 2	0.32[c]
OTC resistant (n = 4)				
R1	32–64	8–16	64 & 0.25	1.36
F1	32	8–16	16 & 4	1.00
M1	16–64	8	32 & 4	1.25
T1	32–64	8	32 & 4	1.25

[a] Combination of OTC and Bz concentrations yielding the lowest FIC value.[119] [b] The FIC means were calculated based on three replicated experiments for each strain. [c] The FIC value indicates synergistic interaction between OTC and Bz.

leaf feature (Fig. 4D, H, L and P). These images show that despite OTC residue mostly covers the outer periclinal surface of the epidermal cells, which is not usually inhabited by bacteria. Fluorescence micrographs (Fig. 4K and O) confirm that when mixed with Bz, OTC is also preferentially deposited between the epidermal cells and stomata. This demonstrates that Bz preferential deposition is exploitable for targeted delivery of OTC and perhaps similar agrochemicals in general. Additionally, the saplings were observed 72 hours after foliar application (Fig. S8†) to ensure that the treatments did not cause acute toxicity to plant tissue. It was observed that treated plants did not exhibit any necrotic lesions, leaf burn, or defoliation, suggesting Bz and Bz–OTC materials are safe (non-phytotoxic). Further longitudinal studies are needed to confirm if leaf expansion, respiration or chlorophyll content are not negatively impacted because of the preferential deposition around and inside the stomata and between epidermal cells.

Checkerboard Bz–OTC

The MIC of OTC ranged from 0.125–2 μg mL^{-1} for the sensitive strain (2WF91) and 16–64 μg mL^{-1} for the resistant strains (R1, M1, T1, and F1). The MIC of Bz ranged from 8–16 μg of Zn mL^{-1} for both sensitive and resistant strains (Fig. 5). An additive effect was observed for the two bactericides (Bz and OTC) in all the experiments, except for $MIC_{OTC\ combination}$ & $MIC_{Bz\ combination}$ of 0.0625 and 2 μg mL^{-1} where synergism was detected (FIC = 0.3281) (Table 2).

Bz exhibited significant antimicrobial potency against all tested Xap strains and no phytotoxicity up to 800 μg of Zn mL^{-1}. Therefore, it has strong potential for the management of bacterial spot on peach. Furthermore, Bz–OTC will likely slow down the development of resistant genes in OTC-sensitive populations through an enhanced antimicrobial potency and additional mode of action from Zn.

Conclusions

The synthesized boron–zinc nanoformulation exhibited an affinity for the epidermal junction and stomata of peach saplings. This property was exploited for the targeted delivery of OTC to these specific areas. Moreover, Bz–OTC nearly doubled the leaf surface coverage compared to OTC alone. This suggests that Bz–OTC could improve performance *in planta* compared to OTC only. Antimicrobial studies demonstrated that Bz inhibits the growth of OTC sensitive and resistant strains of Xap at very low concentrations. Additionally, Bz–OTC showed synergistic or additive effect in antimicrobial potency, depending on the Xap strain. These findings suggest that Bz–OTC is a more effective tool than OTC alone for managing bacterial spot of peach saplings. Furthermore, other agrochemicals capable of undergoing transition metal complexation or boron ester formation, such as dithiocarbamates[120–124] or salicylic acid,[100,125,126] could potentially be more efficiently delivered using this foliar targeting strategy. This newly discovered targeting strategy has merits to be translated to other plant systems for managing a wide variety of foliar diseases. Moreover, given that Bz residue presented a similar pattern to that of fluorescent nanoparticle uptake through the cuticular and stomatal pathway,[127] it might increase leaf absorption of pesticides and micronutrients. Further work is underway to assess the effectiveness of targeting strategy on various active ingredient absorption and translocation *in planta*.

In summary, targeted delivery is an active area of research with great potential to increase agrochemical use efficiency and reduce their environmental footprint. In this work, we reported a new foliar targeting strategy for agrochemicals. To demonstrate this strategy, Bz was designed and developed, keeping in mind industry viability and environmental safety. Bz effectively delivered OTC to leaf epidermal cell junction and stomata, the most vulnerable areas for pathogen invasion. Future research is needed to fully understand the specific molecular/particle interactions that cause Bz to preferentially deposit on specific leaf structures. Understanding this mode of action will lead to the development of better targeting delivery systems for agriculture.

Author contributions

Jorge Pereira: conceptualization, methodology, investigation, data curation, formal analysis, visualization, and writing –

original draft, review & editing. Daniela Negrete Moreno: investigation, data curation, formal analysis, visualization, and writing – original draft, review & editing. Giuliana Gan Giannelli: investigation, methodology, validation, and writing – review & editing. Edwin Davidson: investigation, data curation, visualization, writing – review & editing. Javier Rivera-Huertas: investigation, validation and writing – review & editing. Hehe Wang: conceptualization, data curation, formal analysis, funding acquisition, project administration, supervision, and writing – review & editing. Swadeshmukul Santra: conceptualization, funding acquisition, project administration, supervision, and writing – review & editing.

Conflicts of interest

The authors of this work declare no conflict of interest.

Acknowledgements

This work was partly supported by the USDA National Institute of Food and Agriculture, Specialty Crops Research Initiative, grant no. 2021-67013-33574 and SC-1700592. The authors thank Jeffrey Hopkins for supplying the peach saplings. The material SEM-EDS mapping was completed at the Material Characterization Facility of the University of Central Florida - Advanced Materials Processing and Analysis Center.

References

1 S. Savary, A. Ficke, J.-N. Aubertot and C. Hollier, Crop losses due to diseases and their implications for global food production losses and food security, *Food Secur.*, 2012, **4**, 519–537.
2 W. Zhang, Global pesticide use: Profile, trend, cost/benefit and more, *Proc. Int. Acad. Ecol. Environ. Sci.*, 2018, **8**, 1.
3 G. V. Lowry, A. Avellan and L. M. Gilbertson, Opportunities and challenges for nanotechnology in the agri-tech revolution, *Nat. Nanotechnol.*, 2019, **14**, 517–522.
4 Z. Hu, What Socio-Economic and Political Factors Lead to Global Pesticide Dependence? A Critical Review from a Social Science Perspective, *Int. J. Environ. Res. Public Health*, 2020, **17**, 8119.
5 M. J. L. Castro, C. Ojeda and A. F. Cirelli, Advances in surfactants for agrochemicals, *Environ. Chem. Lett.*, 2014, **12**, 85–95.
6 M. Fagnano, D. Agrelli, A. Pascale, P. Adamo, N. Fiorentino, C. Rocco, O. Pepe and V. Ventorino, Copper accumulation in agricultural soils: Risks for the food chain and soil microbial populations, *Sci. Total Environ.*, 2020, **734**, 139434.
7 M. Tudi, H. Daniel Ruan, L. Wang, J. Lyu, R. Sadler, D. Connell, C. Chu and D. T. Phung, Agriculture Development, Pesticide Application and Its Impact on the Environment, *Int. J. Environ. Res. Public Health*, 2021, **18**, 1112.
8 B. Kurenbach, D. Marjoshi, C. F. Amábile-Cuevas, G. C. Ferguson, W. Godsoe, P. Gibson and J. A. Heinemann, Sublethal Exposure to Commercial Formulations of the Herbicides Dicamba, 2,4-Dichlorophenoxyacetic Acid, and Glyphosate Cause Changes in Antibiotic Susceptibility in Escherichia coli and Salmonella enterica serovar Typhimurium, *MBio*, 2015, **6**, 9–15.
9 P. S. Jørgensen, C. Folke, P. J. G. Henriksson, K. Malmros, M. Troell and A. Zorzet, Coevolutionary Governance of Antibiotic and Pesticide Resistance, *Trends Ecol. Evol.*, 2020, **35**, 484–494.
10 P. M. M. Martins, M. V. Merfa, M. A. Takita and A. A. De Souza, Persistence in Phytopathogenic Bacteria: Do We Know Enough?, *Front. Microbiol.*, 2018, **9**, 1099.
11 S. Timilsina, N. Potnis, E. A. Newberry, P. Liyanapathiranage, F. Iruegas-Bocardo, F. F. White, E. M. Goss and J. B. Jones, Xanthomonas diversity, virulence and plant–pathogen interactions, *Nat. Rev. Microbiol.*, 2020, **18**, 415–427.
12 E. Stefani, Economic significance and control of bacterial spot/canker of stone fruits caused by Xanthomonas arboricola pv. pruni, *J. Plant Pathol.*, 2010, **92**, S99–S103.
13 J. R. Lamichhane and L. Varvaro, Xanthomonas arboricola disease of hazelnut: current status and future perspectives for its management, *Plant Pathol.*, 2014, **63**, 243–254.
14 J. Garita-Cambronero, A. Palacio-Bielsa and J. Cubero, Xanthomonas arboricola pv. pruni, causal agent of bacterial spot of stone fruits and almond: its genomic and phenotypic characteristics in the X. arboricola species context, *Mol. Plant Pathol.*, 2018, **19**, 2053–2065.
15 A. Herbert, C. N. Hancock, B. Cox, G. Schnabel, D. Moreno, R. Carvalho, J. Jones, M. Paret, X. Geng and H. Wang, Oxytetracycline and Streptomycin Resistance Genes in Xanthomonas arboricola pv. pruni, the Causal Agent of Bacterial Spot in Peach, *Front. Microbiol.*, 2022, **13**, 821808.
16 A. Kawaguchi, K. Inoue and Y. Inoue, Biological control of bacterial spot on peach by nonpathogenic Xanthomonascampestris strains AZ98101 and AZ98106, *J. Gen. Plant Pathol.*, 2014, **80**, 158–163.
17 B. M. Cox, H. Wang and G. Schnabel, Copper Tolerance in Xanthomonas arboricola pv. pruni in South Carolina Peach Orchards, *Plant Dis.*, 2022, **106**, 1626–1631.
18 N. Lalancette, L. L. Blaus and P. Engel, Refinement of Peach Cover Spray Programs for Management of Brown Rot at Harvest, *Plant Dis.*, 2020, **104**, 1527–1533.
19 D. Wang, N. B. Saleh, A. Byro, R. Zepp, E. Sahle-Demessie, T. P. Luxton, K. T. Ho, R. M. Burgess, M. Flury, J. C. White and C. Su, Nano-enabled pesticides for sustainable agriculture and global food security, *Nat. Nanotechnol.*, 2022, **17**, 347–360.
20 D. Richard, N. Tribot, C. Boyer, M. Terville, K. Boyer, S. Javegny, M. Roux-Cuvelier, O. Pruvost, A. Moreau, A. Chabirand and C. Vernière, First Report of Copper-resistant Xanthomonas citri pv. citri Pathotype A Causing Asiatic Citrus Canker in Réunion, France, *Plant Dis.*, 2017, **101**, 503.
21 A. M. Gochez, J. C. Huguet-Tapia, G. V. Minsavage, D. Shantaraj, N. Jalan, A. Strauss, T. Lahaye, W. Nian, B. I.

Canteros, J. B. Jones and N. Potnis, Pacbio sequencing of copper-tolerant Xanthomonas citri reveals presence of a chimeric plasmid structure and provides insights into reassortment and shuffling of transcription activator-like effectors among X. citri strains, *BMC Genomics.*, 2018, **19**, 16.

22 J. M. Klein-Gordon, Y. Xing, K. A. Garrett, P. Abrahamian, M. L. Paret, G. V. Minsavage, A. L. Strayer-Scherer, J. C. Fulton, S. Timilsina, J. B. Jones, E. M. Goss and G. E. Vallad, Assessing Changes and Associations in the Xanthomonas perforans Population Across Florida Commercial Tomato Fields *Via* a Statewide Survey, *Phytopathology*, 2021, **111**, 1029–1041.

23 Z. Huang, P. Rajasekaran, A. Ozcan and S. Santra, Antimicrobial Magnesium Hydroxide Nanoparticles As an Alternative to Cu Biocide for Crop Protection, *J. Agric. Food Chem.*, 2018, **66**, 8679–8686.

24 Y. Y. Liao, A. Strayer-Scherer, J. C. White, R. De La Torre-Roche, L. Ritchie, J. Colee, G. E. Vallad, J. Freeman, J. B. Jones and M. L. Paret, Particle-size dependent bactericidal activity of magnesium oxide against Xanthomonas perforans and bacterial spot of tomato, *Sci. Rep.*, 2019, **9**, 1–10.

25 Y.-Y. Liao, Y. Huang, R. Carvalho, M. Choudhary, S. Da Silva, J. Colee, A. Huerta, G. E. Vallad, J. H. Freeman, J. B. Jones, A. Keller and M. L. Paret, Magnesium Oxide Nanomaterial, an Alternative for Commercial Copper Bactericides: Field-Scale Tomato Bacterial Spot Disease Management and Total and Bioavailable Metal Accumulation in Soil, *Environ. Sci. Technol.*, 2021, **55**, 13561–13570.

26 X. Cao, C. Wang, X. Luo, L. Yue, J. C. White, W. Elmer, O. P. Dhankher, Z. Wang and B. Xing, Elemental Sulfur Nanoparticles Enhance Disease Resistance in Tomatoes, *ACS Nano*, 2021, **15**, 11817–11827.

27 S. Roy Choudhury, M. Ghosh, A. Mandal, D. Chakravorty, M. Pal, S. Pradhan and A. Goswami, Surface-modified sulfur nanoparticles: an effective antifungal agent against Aspergillus niger and Fusarium oxysporum, *Appl. Microbiol. Biotechnol.*, 2011, **90**, 733–743.

28 Y. H. Kim, G. H. Kim, K. S. Yoon, S. Shankar and J.-W. Rhim, Comparative antibacterial and antifungal activities of sulfur nanoparticles capped with chitosan, *Microb. Pathog.*, 2020, **144**, 104178.

29 S. Shankar, L. Jaiswal and J.-W. Rhim, New insight into sulfur nanoparticles: Synthesis and applications, *Crit. Rev. Environ. Sci. Technol.*, 2020, 1–28.

30 A. Strayer-Scherer, Y. Y. Liao, M. Young, L. Ritchie, G. E. Vallad, S. Santra, J. H. Freeman, D. Clark, J. B. Jones and M. L. Paret, Advanced Copper Composites Against Copper-Tolerant Xanthomonas perforans and Tomato Bacterial Spot, *Phytopathology*, 2017, **108**, 196–205.

31 J. Borgatta, C. Ma, N. Hudson-Smith, W. Elmer, C. D. Plaza Pérez, R. De La Torre-Roche, N. Zuverza-Mena, C. L. Haynes, J. C. White and R. J. Hamers, Copper Based Nanomaterials Suppress Root Fungal Disease in Watermelon (Citrullus lanatus): Role of Particle Morphology, Composition and Dissolution Behavior, *ACS Sustainable Chem. Eng.*, 2018, **6**, 14847–14856.

32 W. Elmer, R. De La Torre-Roche, L. Pagano, S. Majumdar, N. Zuverza-Mena, C. Dimkpa, J. Gardea-Torresdey and J. C. White, Effect of Metalloid and Metal Oxide Nanoparticles on Fusarium Wilt of Watermelon, *Plant Dis.*, 2018, **102**, 1394–1401.

33 D. K. Ghosh, S. Kokane, P. Kumar, A. Ozcan, A. Warghane, M. Motghare, S. Santra and A. K. Sharma, Antimicrobial nano-zinc oxide-2S albumin protein formulation significantly inhibits growth of "Candidatus Liberibacter asiaticus" in planta, *PLoS One*, 2018, **13**, e0204702.

34 R. Carvalho, K. Duman, J. B. Jones and M. L. Paret, Bactericidal Activity of Copper-Zinc Hybrid Nanoparticles on Copper-Tolerant Xanthomonas perforans, *Sci. Rep.*, 2019, **9**, 1–9.

35 A. Ozcan, M. Young, B. Lee, Y.-Y. Liao, S. D. Silva, D. Godden, J. Colee, Z. Huang, H. C. Mendis, M. G. N. Campos, J. B. Jones, J. H. Freeman, M. L. Paret, L. Tetard and S. Santra, Copper-fixed quat: a hybrid nanoparticle for application as a locally systemic pesticide (LSP) to manage bacterial spot disease of tomato, *Nanoscale Adv.*, 2021, **3**, 1473–1483.

36 M. Soliman, B. Lee, A. Ozcan, T. B. Rawal, M. Young, H. C. Mendis, P. Rajasekaran, T. Washington, S. V. Pingali, H. O'Neill, A. Gesquiere, L. D. L. Fuente, L. Petridis, E. Johnson, J. Graham, S. Santra and L. Tetard, Engineered zinc oxide-based nanotherapeutics boost systemic antibacterial efficacy against phloem-restricted diseases, *Environ. Sci.: Nano*, 2022, **9**, 2869–2886.

37 J. Pereira, A. King, M. G. N. Campos and S. Santra, Advanced Copper and Copper Alternatives for Crop Protection - A Mini-Review, *Curr. Nanosci.*, 2022, **18**, 410–424.

38 S. E. Lindow and M. T. Brandl, Microbiology of the Phyllosphere, *Appl. Environ. Microbiol.*, 2003, **69**, 1875–1883.

39 J. A. Vorholt, Microbial life in the phyllosphere, *Nat. Rev. Microbiol.*, 2012, **10**, 828–840.

40 N. Xu, Q. Zhao, Z. Zhang, Q. Zhang, Y. Wang, G. Qin, M. Ke, D. Qiu, W. J. G. M. Peijnenburg, T. Lu and H. Qian, Phyllosphere Microorganisms: Sources, Drivers, and Their Interactions with Plant Hosts, *J. Agric. Food Chem.*, 2022, **70**, 4860–4870.

41 J.-M. Monier and S. E. Lindow, Frequency, Size, and Localization of Bacterial Aggregates on Bean Leaf Surfaces, *Appl. Environ. Microbiol.*, 2004, **70**, 346–355.

42 S. Wani, J. Barnes and I. Singleton, Investigation of potential reasons for bacterial survival on 'ready-to-eat' leafy produce during exposure to gaseous ozone, *Postharvest Biol. Technol.*, 2016, **111**, 185–190.

43 J. Aarrouf, A. Garcin, Y. Lizzi and M. E. Maâtaoui, Immunolocalization and Histocytopathological Effects of Xanthomonas arboricola pv. pruni on Naturally Infected Leaf and Fruit Tissues of Peach (Prunus persica L. Batsch), *J. Phytopathol.*, 2008, **156**, 338–345.

44 Y. Zhang, E. M. Callaway, J. B. Jones and M. Wilson, Visualisation of hrp gene expression in Xanthomonas euvesicatoria in the tomato phyllosphere, *Eur. J. Plant Pathol.*, 2009, **124**, 379–390.
45 J. Cubero, I. Gell, E. G. Johnson, A. Redondo and J. H. Graham, Unstable green fluorescent protein for study of Xanthomonas citri subsp. citri survival on citrus, *Plant Pathol.*, 2011, **60**, 977–985.
46 J. H. J. Leveau and S. E. Lindow, Appetite of an epiphyte: Quantitative monitoring of bacterial sugar consumption in the phyllosphere, *Proc. Natl. Acad. Sci.*, 2001, **98**, 3446–3453.
47 M. N. P. Remus-Emsermann, G. A. Kowalchuk and J. H. J. Leveau, Single-cell *versus* population-level reproductive success of bacterial immigrants to pre-colonized leaf surfaces, *Environ. Microbiol. Rep.*, 2013, **5**, 387–392.
48 M. N. P. Remus-Emsermann, S. Lücker, D. B. Müller, E. Potthoff, H. Daims and J. A. Vorholt, Spatial distribution analyses of natural phyllosphere-colonizing bacteria on Arabidopsis thaliana revealed by fluorescence *in situ* hybridization, *Environ. Microbiol.*, 2014, **16**, 2329–2340.
49 M. N. P. Remus-Emsermann and R. O. Schlechter, Phyllosphere microbiology: at the interface between microbial individuals and the plant host, *New Phytol.*, 2018, **218**, 1327–1333.
50 P. Taylor, The wetting of leaf surfaces, *Curr. Opin. Colloid Interface Sci.*, 2011, **16**, 326–334.
51 R. Bourgault, S. Matschi, M. Vasquez, P. Qiao, A. Sonntag, C. Charlebois, M. Mohammadi, M. J. Scanlon, L. G. Smith and I. Molina, Constructing functional cuticles: analysis of relationships between cuticle lipid composition, ultrastructure and water barrier function in developing adult maize leaves, *Ann. Bot.*, 2020, **125**, 79–91.
52 R. Jetter and M. Riederer, Localization of the Transpiration Barrier in the Epi- and Intracuticular Waxes of Eight Plant Species: Water Transport Resistances Are Associated with Fatty Acyl Rather Than Alicyclic Components, *Plant Physiol.*, 2016, **170**, 921–934.
53 K. H. Caffall and D. Mohnen, The structure, function, and biosynthesis of plant cell wall pectic polysaccharides, *Carbohydr. Res.*, 2009, **344**, 1879–1900.
54 M. Ochoa-Villarreal, E. Aispuro-Hernández, I. Vargas-Arispuro, M. Á. Martínez-Téllez, M. Ochoa-Villarreal, E. Aispuro-Hernández, I. Vargas-Arispuro and M. Á. Martínez-Téllez, *Plant Cell Wall Polymers: Function, Structure and Biological Activity of Their Derivatives*, IntechOpen, 2012.
55 S. Amsbury, L. Hunt, N. Elhaddad, A. Baillie, M. Lundgren, Y. Verhertbruggen, H. V. Scheller, J. P. Knox, A. J. Fleming and J. E. Gray, Stomatal Function Requires Pectin De-methyl-esterification of the Guard Cell Wall, *Curr. Biol.*, 2016, **26**, 2899–2906.
56 X. Sun, I. G. Andrew, P. J. Harris, S. O. Hoskin, K. N. Joblin and Y. He, Mapping Pectic-Polysaccharide Epitopes in Cell Walls of Forage Chicory (Cichorium intybus) Leaves, *Front. Plant Sci.*, 2021, **12**, 762121.
57 W. G. T. Willats, L. McCartney, W. Mackie and J. P. Knox, Pectin: cell biology and prospects for functional analysis, *Plant Mol. Biol.*, 2001, **47**, 9–27.
58 E. Spielman-Sun, A. Avellan, G. D. Bland, E. T. Clement, R. V. Tappero, A. S. Acerbo and G. V. Lowry, Protein coating composition targets nanoparticles to leaf stomata and trichomes, *Nanoscale*, 2020, **12**, 3630–3636.
59 M. A. O'Neill, D. Warrenfeltz, K. Kates, P. Pellerin, T. Doco, A. G. Darvill and P. Albersheim, Rhamnogalacturonan-II, a pectic polysaccharide in the walls of growing plant cell, forms a dimer that is covalently cross-linked by a borate ester. *In vitro* conditions for the formation and hydrolysis of the dimer, *J. Biol. Chem.*, 1996, **271**, 22923–22930.
60 T. Matoh, S. Kawaguchi and M. Kobayashi, Ubiquity of a Borate-Rhamnogalacturonan II Complex in the Cell Walls of Higher Plants, *Plant Cell Physiol.*, 1996, **37**, 636–640.
61 T. Matoh and M. Kobayashi, Boron and calcium, essential inorganic constituents of pectic polysaccharides in higher plant cell walls, *J. Plant Res.*, 1998, **111**, 179–190.
62 D. Chormova and S. C. Fry, Boron bridging of rhamnogalacturonan-II is promoted *in vitro* by cationic chaperones, including polyhistidine and wall glycoproteins, *New Phytol.*, 2016, **209**, 241–251.
63 D. Gawkowska, J. Cybulska and A. Zdunek, Structure-Related Gelling of Pectins and Linking with Other Natural Compounds: A Review, *Polymer*, 2018, **10**, 762.
64 D. Gawkowska, J. Cybulska and A. Zdunek, Cross-linking of sodium carbonate-soluble pectins from apple by zinc ions, *Carbohydr. Polym.*, 2018, **196**, 1–7.
65 T. J. Maxwell, P. Rajasekaran, M. Young, M. Schaff, R. Heetai and S. Santra, Non-phytotoxic zinc based nanoparticle adjuvant for improving rainfastness and sustained release of streptomycin, *Environ. Nanotechnol., Monit. Manage.*, 2020, **14**, 100355.
66 M. Young, A. Ozcan, P. Rajasekaran, P. Kumrah, M. E. Myers, E. Johnson, J. H. Graham and S. Santra, Fixed-Quat: An Attractive Nonmetal Alternative to Copper Biocides against Plant Pathogens, *J. Agric. Food Chem.*, 2018, **66**, 13056–13064.
67 S. L. Smith, M. G. N. Campos, A. Ozcan, H. C. Mendis, M. Young, M. E. Myers, M. Atilola, M. Doomra, Z. Thwin, E. G. Johnson and S. Santra, Multifunctional Surface, Subsurface, and Systemic Therapeutic (MS3T) Formulation for the Control of Citrus Canker, *J. Agric. Food Chem.*, 2021, **69**, 10807–10818.
68 G. C. Schutte, C. Kotze, J. G. van Zyl and P. H. Fourie, Assessment of retention and persistence of copper fungicides on orange fruit and leaves using fluorometry and copper residue analyses, *Crop Prot.*, 2012, **42**, 1–9.
69 J. Xiang, M. Hare, L. Vickers and P. Kettlewell, Estimation of film antitranspirant spray coverage on rapeseed (Brassica napus L.) leaves using titanium dioxide, *Crop Prot.*, 2021, **142**, 105531.
70 S. Pillai, R. Moellering and G. Eliopoulos, Antimicrobial Combinations, *Antibiotics in Laboratory Medicine*, Lippincott Williams & Wilkins, 5th edn, 2005, pp. 374–440.

71 P. Bellio, L. Fagnani, L. Nazzicone and G. Celenza, New and simplified method for drug combination studies by checkerboard assay, *MethodsX*, 2021, **8**, 101543.
72 S. Paria, R. G. Chaudhuri and N. Noah Jason, Self-assembly of colloidal sulfur particles on a glass surface from evaporating sessile drops: influence of different salts, *New J. Chem.*, 2014, **38**, 5943–5951.
73 N. Basu and R. Mukherjee, Evaporative Drying of Sodium Chloride Solution Droplet on a Thermally Controlled Substrate, *J. Phys. Chem. B*, 2020, **124**, 1266–1274.
74 H. Jia, X. Bai and L. Zheng, Facile preparation of CaCO3 nanocrystals with unique morphologies controlled by supramolecular complexes, *CrystEngComm*, 2011, **13**, 7252–7257.
75 J. K. Dewangan, N. Basu and M. Chowdhury, Cationic surfactant-directed structural control of NaCl crystals from evaporating sessile droplets, *Soft Matter*, 2021, **18**, 62–79.
76 A. Sen and B. Ganguly, Is Dual Morphology of Rock-Salt Crystals Possible with a Single Additive? The Answer Is Yes, with Barbituric Acid, *Angew. Chem., Int. Ed.*, 2012, **51**, 11279–11283.
77 X. Guo, L. Liu, W. Wang, J. Zhang, Y. Wang and S.-H. Yu, Controlled crystallization of hierarchical and porous calcium carbonate crystals using polypeptide type block copolymer as crystal growth modifier in a mixed solution, *CrystEngComm*, 2011, **13**, 2054–2061.
78 Y. Qin, D. Yu and J. Zhou, DNA action on the growth and habit modification of NaCl crystals, *CrystEngComm*, 2017, **19**, 5356–5360.
79 B. Pathak, J. Christy, K. Sefiane and D. Gozuacik, Complex Pattern Formation in Solutions of Protein and Mixed Salts Using Dehydrating Sessile Droplets, *Langmuir*, 2020, **36**, 9728–9737.
80 Y. Zhang, X. Cai, X. Lang, X. Qiao, X. Li and J. Chen, Insights into aquatic toxicities of the antibiotics oxytetracycline and ciprofloxacin in the presence of metal: Complexation *versus* mixture, *Environ. Pollut.*, 2012, **166**, 48–56.
81 Y. Zhao, Y. Tan, Y. Guo, X. Gu, X. Wang and Y. Zhang, Interactions of tetracycline with Cd (II), Cu (II) and Pb (II) and their cosorption behavior in soils, *Environ. Pollut.*, 2013, **180**, 206–213.
82 M. Jia, F. Wang, X. Jin, Y. Song, Y. Bian, L. A. Boughner, X. Yang, C. Gu, X. Jiang and Q. Zhao, Metal ion–oxytetracycline interactions on maize straw biochar pyrolyzed at different temperatures, *Chem. Eng. J.*, 2016, **304**, 934–940.
83 H. Chen, J. Peng, L. Yu, H. Chen, M. Sun, Z. Sun, R. Ni, K. A. Alamry, H. M. Marwani and S. Wang, Calcium Ions Turn on the Fluorescence of Oxytetracycline for Sensitive and Selective Detection, *J. Fluoresc.*, 2020, **30**, 463–470.
84 J. A. L. da Silva, Borate esters of polyols: Occurrence, applications and implications, *Inorg. Chim. Acta*, 2021, **520**, 120307.
85 J. A. Peters, Interactions between boric acid derivatives and saccharides in aqueous media: Structures and stabilities of resulting esters, *Coord. Chem. Rev.*, 2014, **268**, 1–22.
86 S. Guieu, C. I. C. Esteves, J. Rocha and A. M. S. Silva, Multicomponent Synthesis of Luminescent Iminoboronates, *Molecules*, 2020, **25**, E6039.
87 Y. Egawa, R. Miki and T. Seki, Colorimetric Sugar Sensing Using Boronic Acid-Substituted Azobenzenes, *Materials*, 2014, **7**, 1201–1220.
88 A. Franco and J. A. L. da Silva, Boron in Prebiological Evolution, *Angewandte Chemie*, 2021, **133**, 10550–10560.
89 C. Boonkanon, K. Phatthanawiwat, W. Wongniramaikul and A. Choodum, Curcumin nanoparticle doped starch thin film as a green colorimetric sensor for detection of boron, *Spectrochim. Acta, Part A*, 2020, **224**, 117351.
90 G. T. Williams, J. L. Kedge and J. S. Fossey, Molecular Boronic Acid-Based Saccharide Sensors, *ACS Sens.*, 2021, **6**, 1508–1528.
91 Y. Hu, L. Shao, Y. Fan, L. Lu, C. Zhou, H. Fu and Y. She, Colorimetric discrimination of tea polyphenols based on boronic acid sensor assembled with pH indicator, *Dyes Pigm.*, 2022, **203**, 110326.
92 J. T. Hatcher and L. V. Wilcox, Colorimetric determination of boron using carmine, *Anal. Chem.*, 1950, **22**, 567–569.
93 M. R. Hayes and J. Metcalfe, The boron-curcumin complex in the determination of trace amounts of boron, *Analyst*, 1962, **87**, 956–969.
94 T. P. Gaines and G. A. Mitchell, Boron determination in plant tissue by the azomethine H method, *Commun. Soil Sci. Plant Anal.*, 1979, **10**, 1099–1108.
95 R. N. Sah and P. H. Brown, Boron Determination—A Review of Analytical Methods, *Microchem. J.*, 1997, **56**, 285–304.
96 T. C. Mohan and A. M. E. Jones, Determination of Boron Content Using a Simple and Rapid Miniaturized Curcumin Assay, *Bio-Protoc.*, 2018, **8**, e2703.
97 F. Pena-Pereira, A. Velázquez, I. Lavilla and C. Bendicho, A paper-based colorimetric assay with non-instrumental detection for determination of boron in water samples, *Talanta*, 2020, **208**, 120365.
98 M. Bishop, N. Shahid, J. Yang and A. R. Barron, Determination of the mode and efficacy of the cross-linking of guar by borate using MAS 11B NMR of borate cross-linked guar in combination with solution 11B NMR of model systems, *Dalton Trans.*, 2004, 2621–2634.
99 C. Chiappe, F. Signori, G. Valentini, L. Marchetti, C. S. Pomelli and F. Bellina, Novel (Glycerol)borate-Based Ionic Liquids: An Experimental and Theoretical Study, *J. Phys. Chem. B*, 2010, **114**, 5082–5088.
100 J. Schott, J. Kretzschmar, S. Tsushima, B. Drobot, M. Acker, A. Barkleit, S. Taut, V. Brendler and T. Stumpf, The interaction of Eu(III) with organoborates – a further approach to understand the complexation in the An/Ln(iii)–borate system, *Dalton Trans.*, 2015, **44**, 11095–11108.
101 J. Schott, J. Kretzschmar, M. Acker, S. Eidner, M. U. Kumke, B. Drobot, A. Barkleit, S. Taut, V. Brendler and T. Stumpf,

Formation of a Eu(III) borate solid species from a weak Eu(III) borate complex in aqueous solution, *Dalton Trans.*, 2014, **43**, 11516–11528.

102 S. A. van Zyl, J.-C. Brink, F. J. Calitz, S. Coertze and P. H. Fourie, The use of adjuvants to improve spray deposition and Botrytis cinerea control on Chardonnay grapevine leaves, *Crop Prot.*, 2010, **29**, 58–67.

103 M. J. Gimenes, H. Zhu, C. G. Raetano and R. B. Oliveira, Dispersion and evaporation of droplets amended with adjuvants on soybeans, *Crop Prot.*, 2013, **44**, 84–90.

104 J. M. Crane and G. C. Bergstrom, Spatial distribution and antifungal interactions of a Bacillus biological control agent on wheat surfaces, *Biol. Control*, 2014, **78**, 23–32.

105 R. B. de Oliveira, L. M. Bonadio Precipito, M. A. Gandolfo, J. V. de Oliveira and F. R. Lucio, Effect of droplet size and leaf surface on retention of 2,4-D formulations, *Crop Prot.*, 2019, **119**, 97–101.

106 L. He, X. Li, Y. Gao, B. Li, W. Mu and F. Liu, Oil Adjuvants Enhance the Efficacy of Pyraclostrobin in Managing Cucumber Powdery Mildew (Podosphaera xanthii) by Modifying the Affinity of Fungicide Droplets on Diseased Leaves, *Plant Dis.*, 2019, **103**, 1657–1664.

107 G. Wang, Y. Lan, H. Yuan, H. Qi, P. Chen, F. Ouyang and Y. Han, Comparison of Spray Deposition, Control Efficacy on Wheat Aphids and Working Efficiency in the Wheat Field of the Unmanned Aerial Vehicle with Boom Sprayer and Two Conventional Knapsack Sprayers, *Appl. Sci.*, 2019, **9**, 218.

108 Q. Xiao, R. Du, L. Yang, X. Han, S. Zhao, G. Zhang, W. Fu, G. Wang and Y. Lan, Comparison of Droplet Deposition Control Efficacy on Phytophthora capsica and Aphids in the Processing Pepper Field of the Unmanned Aerial Vehicle and Knapsack Sprayer, *Agronomy*, 2020, **10**, 215.

109 P. Chen, Y. Lan, X. Huang, H. Qi, G. Wang, J. Wang, L. Wang and H. Xiao, Droplet Deposition and Control of Planthoppers of Different Nozzles in Two-Stage Rice with a Quadrotor Unmanned Aerial Vehicle, *Agronomy*, 2020, **10**, 303.

110 K. Adusei-Fosu, C. A. Rolando, B. Richardson, R. van Leeuwen, R. Gaskin, M. K.-F. Bader and A. K. Pathan, Evaluating the efficacy of potential fungicide-adjuvant combinations for control of myrtle rust in New Zealand, *J. Plant Dis. Prot.*, 2021, **128**, 1501–1515.

111 E. Cerruto, G. Manetto, D. Longo, S. Failla and R. Papa, A model to estimate the spray deposit by simulated water sensitive papers, *Crop Prot.*, 2019, **124**, 104861.

112 R. F. Menger, M. Bontha, J. R. Beveridge, T. Borch and C. S. Henry, Fluorescent Dye Paper-Based Method for Assessment of Pesticide Coverage on Leaves and Trees: A Citrus Grove Case Study, *J. Agric. Food Chem.*, 2020, **68**, 14009–14014.

113 L. A. Palladini, C. G. Raetano and E. D. Velini, Choice of tracers for the evaluation of spray deposits, *Sci. Agric.*, 2005, **62**, 440–445.

114 E. Hilz and A. W. P. Vermeer, Spray drift review: The extent to which a formulation can contribute to spray drift reduction, *Crop Prot.*, 2013, **44**, 75–83.

115 Best Practices for Effective Spraying In Orchards and Vineyards, **https://ohioline.osu.edu/factsheet/fabe-539**, (accessed 3 September 2022).

116 Spray coverage is key for effective treatment results in greenhouse, **https://www.canr.msu.edu/news/spray_coverage_is_key_for_effective_treatment_results_in_greenhouse**, (accessed 3 September 2022).

117 R. D. Deegan, O. Bakajin, T. F. Dupont, G. Huber, S. R. Nagel and T. A. Witten, Capillary flow as the cause of ring stains from dried liquid drops, *Nature*, 1997, **389**, 827–829.

118 A. Kaliyaraj Selva Kumar, Y. Zhang, D. Li and R. G. Compton, A mini-review: How reliable is the drop casting technique?, *Electrochem. Commun.*, 2020, **121**, 106867.

119 C. Palmieri, M. Vecchi, P. Littauer, A. Sundsfjord, P. E. Varaldo and B. Facinelli, Clonal Spread of Macrolide- and Tetracycline-Resistant [erm(A) tet(O)] emm77 Streptococcus pyogenes Isolates in Italy and Norway, *Antimicrob. Agents Chemother.*, 2006, **50**, 4229–4230.

120 L. Yang, X. Zhang, J. Wang, H. Sun and L. Jiang, Double-decrease of the fluorescence of CdSe/ZnS quantum dots for the detection of zinc(II) dimethyldithiocarbamate (ziram) based on its interaction with gold nanoparticles, *Microchim. Acta*, 2018, **185**, 472.

121 H.-U. Islam, A. Roffey, N. Hollingsworth, W. Bras, G. Sankar, N. H. D. Leeuw and G. Hogarth, Understanding the role of zinc dithiocarbamate complexes as single source precursors to ZnS nanomaterials, *Nanoscale Adv.*, 2020, **2**, 798–807.

122 P. Fanjul-Bolado, R. Fogel, J. Limson, C. Purcarea and A. Vasilescu, Advances in the Detection of Dithiocarbamate Fungicides: Opportunities for Biosensors, *Biosensors*, 2021, **11**, 12.

123 Q. Yang, K. Olaifa, F. P. Andrew, P. A. Ajibade, O. M. Ajunwa and E. Marsili, Assessment of physiological and electrochemical effects of a repurposed zinc dithiocarbamate complex on Acinetobacter baumannii biofilms, *Sci. Rep.*, 2022, **12**, 11701.

124 X. Yang, X. Hu, L. Kong and X. Peng, Selective recovery of Cu(II) from strongly acidic wastewater by zinc dimethyldithiocarbamate: Affecting factors, efficiency and mechanism, *J. Environ. Sci.*, 2023, **129**, 115–127.

125 A. Queen, The kinetics of the reaction of boric acid with salicylic acid, *Can. J. Chem.*, 1977, **55**, 3035–3039.

126 D. A. Köse, B. Zümreoglu-Karan, T. Hökelek and E. Şahin, Boric acid complexes with organic biomolecules: Mono-chelate complexes with salicylic and glucuronic acids, *Inorg. Chim. Acta*, 2010, **363**, 4031–4037.

127 P. Hu, J. An, M. M. Faulkner, H. Wu, Z. Li, X. Tian and J. P. Giraldo, Nanoparticle Charge and Size Control Foliar Delivery Efficiency to Plant Cells and Organelles, *ACS Nano*, 2020, **14**, 7970–7986.

